

TUTDoR

Robot dynamic model: freudenstein-based optimal trajectory and parameter identification.

Item Type	Article
Authors	Ogbemhe, John;Mpofu, Khumbulani;Mokakabye, Mabolaya
DOI	https://doi.org/10.1080/23311916.2022.2046682
Publisher	Taylor and Francis Group
Rights	Attribution-NonCommercial-ShareAlike 4.0 International
Download date	2026-03-11 22:54:40
Item License	http://creativecommons.org/licenses/by-nc-sa/4.0/
Link to Item	https://hdl.handle.net/20.500.14519/1382



Robot dynamic model: freudenstein-based optimal trajectory and parameter identification

John Ogbemhe, Khumbulani Mpofu & Mabolaya Mokakabye |

To cite this article: John Ogbemhe, Khumbulani Mpofu & Mabolaya Mokakabye | (2022) Robot dynamic model: freudenstein-based optimal trajectory and parameter identification, Cogent Engineering, 9:1, 2046682, DOI: [10.1080/23311916.2022.2046682](https://doi.org/10.1080/23311916.2022.2046682)

To link to this article: <https://doi.org/10.1080/23311916.2022.2046682>



© 2022 The Author(s). This open access article is distributed under a Creative Commons Attribution (CC-BY) 4.0 license.



Published online: 21 Mar 2022.



Submit your article to this journal [↗](#)



Article views: 1220



View related articles [↗](#)



View Crossmark data [↗](#)



Citing articles: 3 View citing articles [↗](#)



Received: 15 October 2021
Accepted: 18 February 2022

*Corresponding author: john Ogbemhe, Industrial Engineering, Tshwane University of Technology South Africa
E-mail: johnogbemhe@gmail.com

Reviewing editor:
James Lam, Department of Mechanical Engineering, University of Hong Kong, Hong Kong

Additional information is available at the end of the article

SYSTEMS & CONTROL | RESEARCH ARTICLE

Robot dynamic model: freudenstein-based optimal trajectory and parameter identification

John Ogbemhe^{1*}, Khumbulani Mpfu¹ and Mabolaya Mokakabye¹

Abstract: A thorough understanding of an industrial robot's dynamic model is critical for practical robotic applications. An effective dynamic model is required for optimal controller design and trajectory planning. Robot manufacturers only provide kinematic data, which can only guarantee a certain level of positioner accuracy. The design of the trajectory-planning scheme, on the other hand, necessitates a thorough understanding of its dynamic features. The identification of dynamic parameters involves several procedures. This study used the Euler-Lagrangian equation to derive the robot dynamic model in its canonical form. To excite each link of the irb1600 robot industrial robot while avoiding displacement, velocity, and acceleration discontinuities at the start and endpoints, a Freudenstein 1-3-5 trajectory based on Fourier series expansion was used. The dynamic parameters were determined using the nonlinear least-squares approach based on the Levenberg-Marquart equation. The Savitzky-Golay smoothing filters improved the identification method by decreasing system noise.

Subjects: Industrial Engineering & Manufacturing; Mechanical Engineering; Manufacturing Engineering; Systems & Control Engineering

Keywords: Dynamic model; parameters identification; industrial robotic; manipulators; nonlinear least square; Savitzky-Golay filters

ABOUT THE AUTHOR

The authors are members of the Gibela Research Chair in Manufacturing and Skills Development at Tshwane University of Technology, South Africa. The research chair is led by Prof. K Mpfu. The team's research cuts across the following niche areas: Expert Systems, Artificial Intelligence, Robotics in Manufacturing and Mechatronics, Virtual Commissioning Systems, and ROS-I applications are all being used to improve manufacturing. The team is involved in numerous projects: merSETA Localisation Project For Incubation And Skills Development; Virtual Commissioning in Transport Manufacturing Enterprises; Demanufacturing Research focusing on the locomotive; Smart Mobility Systems; and the Smart Factory Project.

PUBLIC INTEREST STATEMENT

A thorough understanding of an industrial robot's dynamic model is critical for practical robotic applications. An effective dynamic model is required for optimal controller design and trajectory planning. This study used the Euler-Lagrangian equation to derive the robot dynamic model in its canonical form. To excite each link of the irb1600 robot industrial robot while avoiding displacement, velocity, and acceleration discontinuities at the start and endpoints, a Freudenstein 1-3-5 trajectory based on Fourier series expansion was used. The dynamic parameters were determined using the nonlinear least-squares approach based on the Levenberg-Marquart equation. Therefore, a deep understanding and the identification of the base parameters can be used to develop an advanced path planning scheme and model-based controller. The requirement to identify the dynamic robot model stems from a lack of understanding of the robot model characteristics, which results in an inaccurate dynamic model and realistic simulation with practical implications.

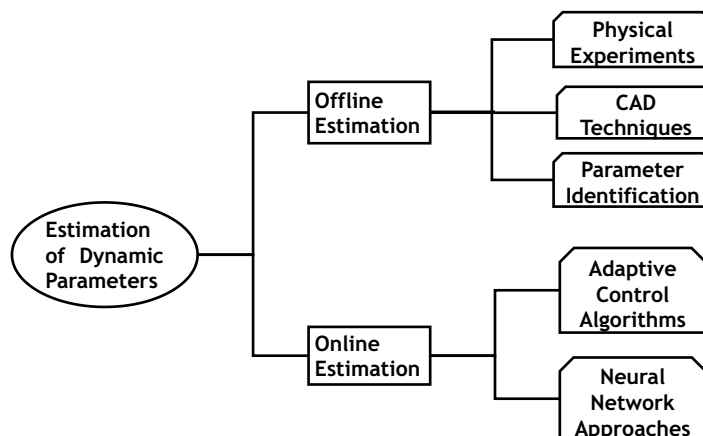
1. Introduction

Robotic applications' usefulness in production is contingent on the accuracy of its tip, owing to the need for precise tracking at high speeds. Numerous variables influence the accuracy and dynamic performance of industrial robots: joint friction, tracking errors of the controller, tolerance in the machining, drive nonlinearities and flexibilities in the drives and joints (Carvalho Bittencourt, 2014; Gautier & Briot, 2013; Hardeman, 2008; Madsen, 2020; Pagani et al., 2020; Sweet & Good, 1985; Villagrossi et al., 2014). Therefore, a deep understanding and the identification of the base parameters can be used to develop an advanced path planning scheme and model-based controller. In robot manipulators, identification is divided into two categories: identifying the robot's kinematic structure and detecting the inertial characteristics of the linkages, actuators, and unknown load the robot carries (Kozlowski, 2012). To effectively deploy robotic techniques in manufacturing, as outlined in (Ogbemhe & Mpfu, 2015; Ogbemhe et al., 2019), a good understanding of the underlying kinematic and dynamic characteristics is required. System identification is the general field concerned with identifying models from measurements (Siciliano & Khatib, 2008). There are two models for system identification: parametric and non-parametric models. Non-parametric models are for complex systems where a few lumped parameters represent the system, whereas parametric models describe many parameters. Parametric models are ideal for manipulators since they are controllable and feature human-made components. The requirement to identify the dynamic robot model stems from a lack of understanding of the robot model characteristics, which results in an inaccurate dynamic model and realistic simulation with practical implications.

There are various works of literature on the estimate of industrial robot dynamic parameters (Ding et al., 2015; Hao et al., 2021; Liu et al., 2021; Madsen, 2020; Pagani et al., 2020); these methods are classed as offline and online estimation strategies (see, Figure 1).

Physical experimentation, computer-aided design (CAD), and parameter identification are examples of offline estimation methods. The online estimation technique uses advanced adaptive control and neural network algorithms. On the other hand, the online estimating technique employs sophisticated adaptive control and neural network technologies. For example, Shang and Cong (2015) demonstrated that parallel robots could enhance tracking accuracy by identifying and calibrating two degrees of freedom. These parameters may now be calculated from robot CAD models by leveraging the capabilities of contemporary CAD software, which is continually expanding. Several researchers have expressed an interest in identifying dynamic parameters. The authors of Gao et al. (2018) employed singular value decomposition (SVD) to identify linearly dependent robotic structural parameters and created an identification strategy that avoids being trapped in a local minimum. Gautier and Briot (2013) studied the use of the Power Identification Model to

Figure 1. Dynamic parameter estimation methods (readapted from (Wu et al., 2010; Zollo et al., 2015).



detect robot inertial parameters by constructing a block-triangular observation matrix using optimised trajectories. Using a non-gradient technique in dynamic parameter identification is becoming more prevalent.

Developing an ideal robot excitation trajectory requires nonlinear optimisation with motion constraints: limitations on the joint angle, velocity, acceleration, and the robot end-effector pose in Cartesian space to avoid colliding with the environment. Numerous ways have been advanced; they all utilised a different method for parameterising the trajectory. For example, in Ding et al. (2015), the authors used an artificial bee colony technique to discover unknown parameters. They validated their strategy using torque prediction accuracy. The method of excitation utilised to excite the robot trajectory is critical in establishing its dynamic properties. Polynomial Huang et al. (2018); trigonometry Chiddarwar and Babu (2012); and exponential Rymanis et al. (2013) trajectories are commonly used in the literature to excite industrial robots. Rackl et al. (2012) suggested using B-splines to excite a seven-jointed DLR Light-Weight Robot equipped with torque sensors in each joint trajectory for dynamic parameter identification studies. The quintic trajectory was used to excite each joint. robot KUKA-iiwaR800 (Hayat, Abhishek, & Saha). In the work of Song et al. (2021), the authors demonstrated the effectiveness of the quintic, polynomial interpolation excitation approach in resolving the nonlinearity and uncertainty issues associated with robot manipulator with a large degree of freedom. Nguyen and Huang (2019) used a single polynomial to excite the trajectory and optimised travelling time.

However, in some cases, these approaches cannot minimise the amplitude of the acceleration profile to reduce effort on the load caused by the vibrational effects of the mechanical structure. Also, a discontinuous acceleration profile lowers the peak of acceleration but may induce oscillations and vibrations due to the corresponding discontinuity of the inertial forces. Furthermore, using Fourier series expansion trajectories can lower the amplitude of the acceleration profile while ensuring the continuity of the position profile and its derivatives up to a specific order (Biagiotti & Melchiorri, 2008).

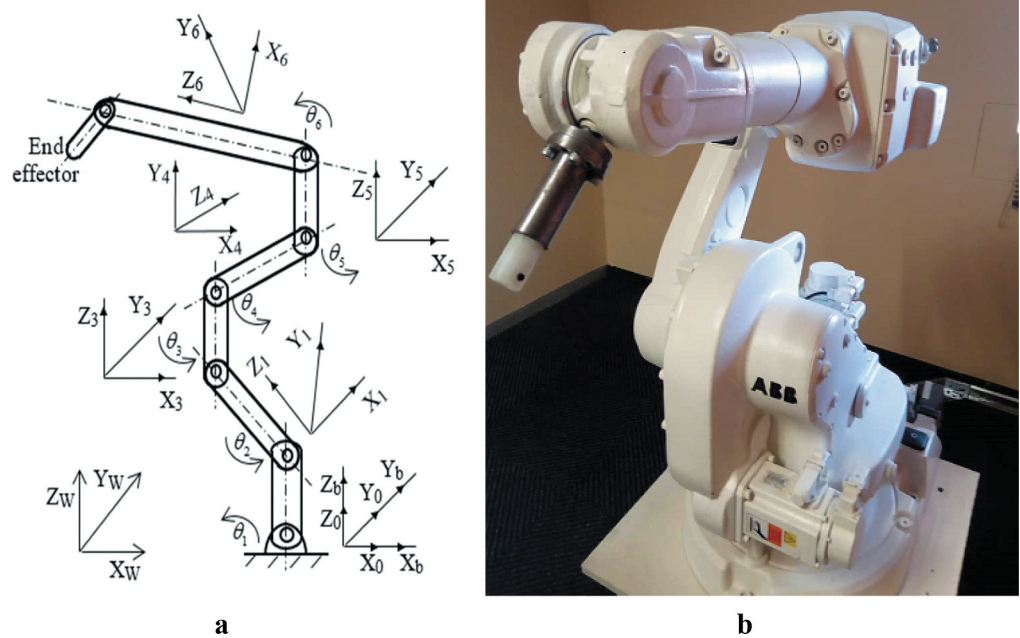
A robust identification model requires optimality criteria during excitation. Kröger (2010), Jin and Gans (2015) proposed Hadamard's inequality to optimise excitation trajectory using an understandable and straightforward criterion. Villagrossi et al. (2014) offer an index for analysing correlation influence among critical parameters under kinematic coupling limitations to determine optimal excitation patterns. Ding et al. (2015) used a fifth-order Fourier series as an excitation trajectory by minimising the minimal condition number. In a related effort, an ideal excitation trajectory for a DLR Light-Weight Robot was described as a restricted optimisation problem using parameterised B-splines (Rackl et al., 2012). The weighted square (Calanca et al., 2010) and least square methods (Rackl et al., 2012) have been widely employed for parameter estimation in industrial robotics. However, while the least square technique produces a more straightforward calculation, it is sensitive to measurement noise and necessitates data pre-processing. The weighted least squares approach, on the other hand, handles issues that are sensitive to noise.

This study derives the robot dynamic model in its canonical form. The industrial robot is excited using a Freudenstein 1-3-5 based optimal trajectory and parameter identification. The use of more Fourier series expansion terms in the Freudenstein 1-3-5 results in profiles with slower acceleration but higher frequency components during excitation. The remainder of the paper is organised as follows. Section 2 discusses the formulation of the dynamic robot model. Sections 3 and 4 deal with the dynamic identification model and experimental validation.

2. Robot dynamic model

The robotic manipulator is defined by each link's kinematic and dynamic parameters. The dynamic model is derived using the theory of generalised coordinates and a scalar function known as the Lagrangian; it contains the difference between the mechanical system's kinetic and potential energy. As a result, an accurate dynamic model is required for robot identification. Figure 2a

Figure 2. (a) industrial robot coordinate systems (b); the industrial robot's structure.



illustrates the ABB irb1600 schematic and coordinates frame. Figure 2b displays the structure of an industrial robot. The Denavit Hartenberg (DH) specifications of the robot are shown in Table 1.

This study aims to present a parameter identification approach, which can correct for the uncertainties in the robotic system during excitation. First, it is mentioned that the examined robot is with 6 degrees of freedom (DOF), which is coupled in series. Moreover, the primary objective of this work is to present a Freudenstein 1-3-5 trajectory, built on the foundation of Fourier series expansion, which was used to excite each link of the industrial robot. A slower acceleration rate is achieved in the Freudenstein 1-3-5 profiles due to the increased usage of Fourier series expansion terms.

The dynamic equation of the industrial robot can be derived from the Lagrange-Euler formulation. It is written in matrix form as

$$\tau = \mathbf{M}(\theta)\ddot{\theta} + \mathbf{H}(\theta, \dot{\theta}) + \tau_f(\theta, \dot{\theta}) + \mathbf{G}(\theta) \tag{1}$$

where $\theta(t) = [\theta_1(t), \theta_2(t), \theta_3(t), \theta_4(t), \theta_5(t), \theta_6(t)]^T \in \mathbb{R}^n$ is a vector of position, and $\dot{\theta}(t) \in \mathbb{R}^n$ $\ddot{\theta}(t) \in \mathbb{R}^n$ are the joint velocity and the acceleration vectors, respectively. $\mathbf{M}(\theta) \in \mathbb{R}^{n \times n}$ is the inertia matrix of the industrial robot, $\mathbf{H}(\theta, \dot{\theta})$ contains Coriolis and centrifugal terms. $\mathbf{G}(\theta)$ is the gravity force terms,

Table 1. The ABB irb1600 industrial robot's Denavit Hartenberg parameters

Linkage	$\alpha_i(^{\circ})$	$a_i(mm)$	$d_i(mm)$	$\theta_i(^{\circ})$
1	-90	150	486.5	θ_1
2	-90	150	486.5	θ_1
3	0	475	0	θ_2
4	-90	0	0	θ_4
5	90	0	0	θ_5
6	0	0	65.0	θ_6

$\tau_f(t) \in \mathbb{R}^n$ is the friction forces and $\tau(t) \in \mathbb{R}^n$ represents the joint torque vector that is the input to the system. The friction force is modelled as

$$\tau_f = f_v \dot{\theta} + f_c \text{sgn}(\dot{\theta}) \tag{2}$$

where the f_v and f_c are constants $n \times n$ diagonal matrices representing viscous and Coulomb friction parameters, respectively, and $\text{sgn}(\cdot)$ is the sign function. The dynamics of the entire six-axis robot can be modelled by:

$$\begin{bmatrix} \tau_1 \\ \tau_2 \\ \tau_3 \\ \tau_4 \\ \tau_5 \\ \tau_6 \end{bmatrix} = \begin{bmatrix} M_{11} & M_{12} & M_{13} & M_{14} & M_{15} & M_{16} \\ M_{21} & M_{22} & M_{23} & M_{24} & M_{25} & M_{26} \\ M_{31} & M_{32} & M_{33} & M_{34} & M_{35} & M_{36} \\ M_{41} & M_{42} & M_{43} & M_{44} & M_{45} & M_{46} \\ M_{51} & M_{52} & M_{53} & M_{54} & M_{55} & M_{56} \\ M_{61} & M_{62} & M_{63} & M_{64} & M_{65} & M_{66} \end{bmatrix} \begin{bmatrix} \ddot{\theta}_1 \\ \ddot{\theta}_2 \\ \ddot{\theta}_3 \\ \ddot{\theta}_4 \\ \ddot{\theta}_5 \\ \ddot{\theta}_6 \end{bmatrix} + \begin{bmatrix} H_1 \\ H_2 \\ H_3 \\ H_4 \\ H_5 \\ H_6 \end{bmatrix} + \begin{bmatrix} \tau_{f1} \\ \tau_{f2} \\ \tau_{f3} \\ \tau_{f4} \\ \tau_{f5} \\ \tau_{f6} \end{bmatrix} + \begin{bmatrix} G_1 \\ G_2 \\ G_3 \\ G_4 \\ G_5 \\ G_6 \end{bmatrix} \tag{3}$$

2.1. Forces acting on the first joint

The dynamic equation for the first link is derived in terms of position and time derivatives in joint space. It takes the following general form in (4) with inertia parameters described in Appendix Table A1.

$$\begin{aligned} \tau_1 = & \ddot{\theta}_1(X_1 + X_2 + X_3 + X_4 + X_5 + X_6) + \ddot{\theta}_2(X_7 + \cos(\theta_1 - \theta_2)(X_8 + X_9 + X_{10} + X_{11}) + X_{12}) \\ & + \ddot{\theta}_3(X_{13} + \cos(\theta_1 - \theta_3)(X_{14} + X_{15} + X_{16} + X_{17})) + \ddot{\theta}_4(X_{18} + \cos(\theta_1 - \theta_4)(X_{19} + X_{20} + X_{21})) \\ & + \ddot{\theta}_5(X_{22} + \cos(\theta_1 - \theta_5)(X_{23} + X_{24})) + \ddot{\theta}_6(X_{25} + \cos(\theta_1 - \theta_6)X_{26}) \\ & + \sin(\theta_1 - \theta_2)(\dot{\theta}_2^2 - \dot{\theta}_1\dot{\theta}_2)(X_{12} + X_{11} + X_{10} + X_9 + X_8) \\ & + \sin(\theta_1 - \theta_3)(\dot{\theta}_3^2 - \dot{\theta}_1\dot{\theta}_3)(X_{17} + X_{16} + X_{15} + X_{14}) \\ & + \sin(\theta_1 - \theta_4)(\dot{\theta}_4^2 - \dot{\theta}_1\dot{\theta}_4)(X_{21} + X_{20} + X_{19}) + \sin(\theta_1 - \theta_5)(\dot{\theta}_5^2 - \dot{\theta}_1\dot{\theta}_5)(X_{24} + X_{23}) \\ & + \sin(\theta_1 - \theta_6)(\dot{\theta}_6^2 - \dot{\theta}_1\dot{\theta}_6)X_{26} + g \cos(\theta_1)X_{27} + \text{sgn}(\dot{\theta}_1)X_{28} + \dot{\theta}_1X_{29} \end{aligned} \tag{4}$$

2.2. Forces acting on the second joint

The dynamic equation for the second link is derived in terms of position and time derivatives in joint space. It takes the following general form in (5) with inertia parameters described in Table A1.

$$\begin{aligned} \tau_2 = & \ddot{\theta}_1(X_7 + \cos(\theta_1 - \theta_2)(X_8 + X_9 + X_{10} + X_{11} + X_{12})) + \ddot{\theta}_2(X_7 + X_{30} + X_{31} + X_{32} + X_{33} + X_{34}) \\ & + \ddot{\theta}_3(X_{13} + \cos(\theta_2 - \theta_3)(X_{35} + X_{36} + X_{37} + X_{38})) + \ddot{\theta}_4(X_{18} + \cos(\theta_2 - \theta_4)(X_{39} + X_{40} + X_{41})) \\ & + \ddot{\theta}_5(X_{22} + \cos(\theta_2 - \theta_5)(X_{42} + X_{43})) + \ddot{\theta}_6(X_{25} + \cos(\theta_2 - \theta_6)X_{44}) \\ & + \sin(\theta_1 - \theta_2)(\dot{\theta}_2^2 - \dot{\theta}_1\dot{\theta}_2)(X_{12} + X_{11} + X_{10} + X_9 + X_8) \\ & + \sin(\theta_2 - \theta_3)(\dot{\theta}_3^2 - \dot{\theta}_2\dot{\theta}_3)(X_{37} + X_{36} + X_{35}) + \sin(\theta_2 - \theta_4)(\dot{\theta}_4^2 - \dot{\theta}_2\dot{\theta}_4)(X_{41} + X_{40} + X_{39}) \\ & + \sin(\theta_2 - \theta_5)(\dot{\theta}_5^2 - \dot{\theta}_2\dot{\theta}_5)(X_{43} + X_{42}) + \sin(\theta_2 - \theta_6)(\dot{\theta}_6^2 - \dot{\theta}_2\dot{\theta}_6)X_{44} \\ & + g \cos \theta_2 X_{45} + \text{sgn}(\dot{\theta}_2)X_{46} + \dot{\theta}_2X_{47} \end{aligned} \tag{5}$$

2.3. Forces acting on the third joint

The dynamic equation for the third link is derived in terms of position and time derivatives in joint space. It takes the following general form in (6) with inertia parameters described in Table A1.

$$\begin{aligned}
 \tau_3 = & \ddot{\theta}_1(X_{18} + \cos(\theta_1 - \theta_3)(X_{14} + X_{15} + X_{16} + X_{17})) \\
 & + \ddot{\theta}_2(X_{18} + \cos(\theta_2 - \theta_3)(X_{35} + X_{36} + X_{37} + X_{38})) \\
 & + \ddot{\theta}_3(X_{18} + X_{48} + X_{49} + X_{50} + X_{51}) + \ddot{\theta}_4(X_{18} + \cos(\theta_3 - \theta_4)(X_{52} + X_{53} + X_{54})) \\
 & + \ddot{\theta}_5(X_{22} + \cos(\theta_3 - \theta_5)(X_{55} + X_{56})) + \ddot{\theta}_6(X_{25} + \cos(\theta_3 - \theta_6)X_{57}) \\
 & + \sin(\theta_1 - \theta_3)(\dot{\theta}_1\dot{\theta}_3 - \dot{\theta}_1^2)(X_{17} + X_{16} + X_{15} + X_{14}) \\
 & + \sin(\theta_2 - \theta_3)(\dot{\theta}_2\dot{\theta}_3 - \dot{\theta}_2^2)(X_{38} + X_{37} + X_{36} + X_{35}) \\
 & + \sin(\theta_3 - \theta_4)(\dot{\theta}_4^2 - \dot{\theta}_3\dot{\theta}_4)(X_{54} + X_{53} + X_{52}) + \sin(\theta_3 - \theta_5)(\dot{\theta}_5^2 - \dot{\theta}_3\dot{\theta}_5)(X_{56} + X_{55}) \\
 & + \sin(\theta_3 - \theta_6)(\dot{\theta}_6^2 - \dot{\theta}_3\dot{\theta}_6)X_{57} + g \cos \theta_3 X_{58} + \operatorname{sgn}(\dot{\theta}_3)X_{59} + \dot{\theta}_3 X_{60}
 \end{aligned} \tag{6}$$

2.4. Forces acting on the fourth joint

The dynamic equation for the fourth link is derived in terms of position and time derivatives in joint space. It takes the following general form in (7) with inertia parameters described in Table A1.

$$\begin{aligned}
 \tau_4 = & \ddot{\theta}_1(X_{18} + \cos(\theta_1 - \theta_4)(X_{19} + X_{20} + X_{21})) + \ddot{\theta}_2(X_{18} + \cos(\theta_2 - \theta_4)(X_{39} + X_{40} + X_{41})) \\
 & + \ddot{\theta}_3(X_{18} + \cos(\theta_3 - \theta_4)(X_{52} + X_{53} + X_{54})) + \ddot{\theta}_4(X_{18} + X_{61} + X_{62} + X_{63}) \\
 & + \ddot{\theta}_5(X_{22} + \cos(\theta_4 - \theta_5)(X_{64} + X_{65})) + \ddot{\theta}_6(X_{25} + \cos(\theta_4 - \theta_6)X_{66}) \\
 & + \sin(\theta_1 - \theta_4)(\dot{\theta}_1\dot{\theta}_4 - \dot{\theta}_1^2)(X_{21} + X_{20} + X_{19}) + \sin(\theta_2 - \theta_4)(\dot{\theta}_2\dot{\theta}_4 - \dot{\theta}_2^2)(X_{41} + X_{40} + X_{39}) \\
 & + \sin(\theta_3 - \theta_4)(\dot{\theta}_3\dot{\theta}_4 - \dot{\theta}_3^2)(X_{54} + X_{53} + X_{52}) + \sin(\theta_4 - \theta_5)(\dot{\theta}_4\dot{\theta}_5 + \dot{\theta}_5^2)(X_{65} + X_{64}) \\
 & + \sin(\theta_4 - \theta_6)(\dot{\theta}_6^2 - \dot{\theta}_4\dot{\theta}_6)X_{66} + g \cos \theta_4 X_{67} + \operatorname{sgn}(\dot{\theta}_4)X_{68} + \dot{\theta}_4 X_{69}
 \end{aligned} \tag{7}$$

2.5. Forces acting on the fifth joint

The dynamic equation for the fifth link is derived in terms of position and time derivatives in joint space. It takes the following general form in (8) with inertia parameters described in Table A1.

$$\begin{aligned}
 \tau_5 = & \ddot{\theta}_1(X_{22} + \cos(\theta_1 - \theta_5)(X_{23} + X_{24})) + \ddot{\theta}_2(X_{22} + \cos(\theta_2 - \theta_5)(X_{42} + X_{43})) \\
 & + \ddot{\theta}_3(X_{22} + \cos(\theta_3 - \theta_5)(X_{56} + X_{57})) + \ddot{\theta}_4(X_{22} + \cos(\theta_4 - \theta_5)(X_{64} + X_{65})) \\
 & + \ddot{\theta}_5(X_{22} + X_{70}) + \ddot{\theta}_6(X_{25} + m_6 \cos(\theta_5 - \theta_6)X_{71}) \\
 & + \sin(\theta_1 - \theta_5)(\dot{\theta}_1\dot{\theta}_5 - \dot{\theta}_1^2)(X_{24} + X_{23}) \\
 & + \sin(\theta_2 - \theta_5)(\dot{\theta}_2\dot{\theta}_5 - \dot{\theta}_2^2)(X_{42} + X_{43}) \\
 & + \sin(\theta_3 - \theta_5)(\dot{\theta}_3\dot{\theta}_5 - \dot{\theta}_3^2)(X_{57} + X_{56}) \\
 & + \sin(\theta_4 - \theta_5)(\dot{\theta}_4\dot{\theta}_5 - \dot{\theta}_4^2)(X_{66} + X_{64}) \\
 & + \sin(\theta_5 - \theta_6)(\dot{\theta}_6^2 - \dot{\theta}_5\dot{\theta}_6)X_{71} \\
 & + g \cos \theta_5 X_{72} + \operatorname{sgn}(\dot{\theta}_5)X_{73} + (\dot{\theta}_5)X_{74}
 \end{aligned} \tag{8}$$

2.6. Forces acting on the sixth joint

The dynamic equation for the sixth link is derived in terms of position and time derivatives in joint space. It takes the following general form in (9) with inertia parameters described in Table A1.

$$\begin{aligned}
 \tau_6 = & \ddot{\theta}_1(X_{25} + \cos(\theta_1 - \theta_6)X_{26}) + \ddot{\theta}_2(X_{25} + \cos(\theta_2 - \theta_6)X_{44}) + \ddot{\theta}_3(X_{25} + \cos(\theta_3 - \theta_6)X_{58}) \\
 & + \ddot{\theta}_4(X_{25} + \cos(\theta_4 - \theta_6)X_{66}) + \ddot{\theta}_5(X_{25} + m_6 \cos(\theta_5 - \theta_6)X_{71}) + \ddot{\theta}_6(X_{25} + X_{75}) \\
 & + \sin(\theta_1 - \theta_6)(\dot{\theta}_1\dot{\theta}_6 - \dot{\theta}_1^2)X_{26} + \sin(\theta_2 - \theta_6)(\dot{\theta}_2\dot{\theta}_6 - \dot{\theta}_2^2)X_{44} \\
 & + \sin(\theta_3 - \theta_6)(\dot{\theta}_3\dot{\theta}_6 - \dot{\theta}_3^2)X_{58} + \sin(\theta_4 - \theta_6)(\dot{\theta}_4\dot{\theta}_6 - \dot{\theta}_4^2)X_{66} \\
 & + \sin(\theta_5 - \theta_6)(\dot{\theta}_5\dot{\theta}_6 - \dot{\theta}_5^2)X_{71} + g \cos \theta_6 X_{76} + \operatorname{sgn}(\dot{\theta}_6)X_{77} + (\dot{\theta}_6)X_{78}
 \end{aligned} \tag{9}$$

3. Dynamic identification model

The complexity of the robot’s dynamic equations makes estimating its parameters problematic. On the other hand, the equations of motion are linear in terms of the inertia parameters. (1) describes the mathematical model in joint space, which may be rewritten as a linearly parameterised form using the DH convention as indicated in (10):

$$\tau = Y(\theta, \dot{\theta}, \ddot{\theta})X \tag{10}$$

where $Y(\theta, \dot{\theta}, \ddot{\theta}) \in \mathbb{R}^{n \times N_s}$ is called the regressor matrix and $X_s \in \mathbb{R}^{N_s \times 1}$ is the standard parameter vector. In summary, Figure 3 illustrates the parameter identification method’s operations; meanwhile, the suggested approximation identification model does not affect the inertia and joint viscous parameters in X dependency on them. Additionally, analogous to the rigid body case, the exciting trajectories may be optimised across the robot’s workspace to mitigate the influence of small perturbations and ensure identification accuracy.

The six components of the inertia matrix, link masses viscous, and column friction coefficients are among the 13 standard parameters for a rigid industrial robot through each link and joint (Jin & Gans, 2015). Furthermore, an excitation reference trajectory is continually used to stimulate the industrial robot. Therefore, we use a Freudenstein 1-3-5 based optimal periodic trajectory in this study. The use of the Freudenstein 1-3-5 based trajectory to excite the industrial robot is motivated by the following:

- It may be advantageous to reduce the amplitude of the acceleration profile to prevent load efforts caused by inertial forces or mechanical structural vibrations.
- A discontinuous acceleration profile lowers the peak of acceleration but may induce vibrations due to the corresponding discontinuity of the inertial forces.
- On the other hand, the cycloidal trajectory has a low harmonic content but has a greater acceleration value.

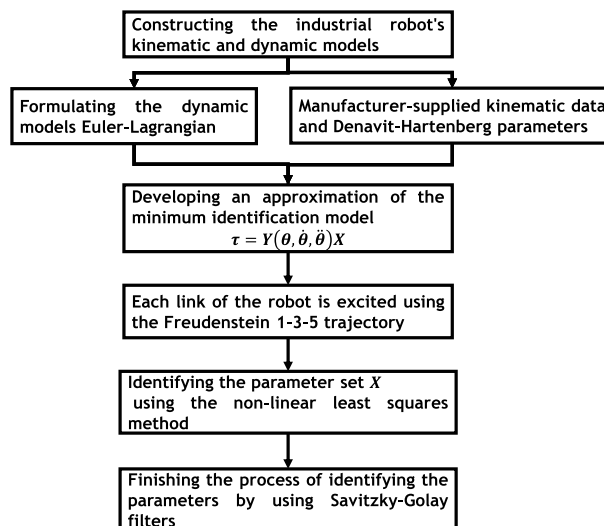
3.1. Nonlinear least square

The nonlinear least square (NLS) problem described in this manuscript is modelled as (Gavin, 2019):

$$X^2(p) = \sum_i^k \left[\frac{y(t_i) - \hat{y}(t_i; p)}{\sigma_{y_i}} \right]^2 = (y - \hat{y}(p))^T W (y - \hat{y}(p)) \tag{11}$$

$$= y^T W y - 2y^T W \hat{y} + \hat{y}^T W \hat{y}$$

Figure 3. The procedure of the parameter identification method.



where $\hat{y}(t_i; p)$ is a model function of an independent variable t and a vector of n parameters p to a set of k data points (t_i, y_i) . The variable W is the weighting matrix and σ_{y_i} is the measurement error for the datum $y(t_i)$.

Because it does not need as many equations as the number of variables, the Levenberg-Marquart technique is employed to construct our nonlinear least square algorithm rather than the Trust-region-reflection approach. Furthermore, the Levenberg-Marquart uses two numerical minimisation techniques: gradient descent and Gauss-Newton, by adaptively altering parameter updates between the two schemes using the update mechanism in the Levenberg-Marquart (12),

$$[J^T W J + \lambda I] h_{lm} = J^T W (y - \hat{y}) \tag{12}$$

where λ is the damping parameter and J is used to denote $\frac{\partial \hat{y}}{\partial p}$.

3.2. Trajectory parametrisation and optimisation

A Freudenstein 1-3-5 trajectory is used to determine the excitation of each link; it is based on Fourier series expansion. The Freudenstein 1-3-5 trajectory was chosen because it minimises the amplitude of the acceleration profile, hence avoiding mechanical structural vibrations. This trajectory is expressed as (Biagiotti & Melchiorri, 2008):

$$\theta(t) = \theta_0 \frac{h(t - t_0)}{T} - \frac{h}{2\pi} \alpha \left(\sin \frac{2\pi(t - t_0)}{T} + \frac{1}{54} \sin \frac{6\pi(t - t_0)}{T} + \frac{1}{1250} \sin \frac{10\pi(t - t_0)}{T} \right) \tag{13}$$

$$\dot{\theta}(t) = \frac{h}{2} \left[1 - \alpha \left(\cos \frac{2\pi(t - t_0)}{T} \right) + \frac{1}{18} \left(\cos \frac{6\pi(t - t_0)}{T} \right) + \frac{1}{250} \left(\cos \frac{10\pi(t - t_0)}{T} \right) \right] \tag{14}$$

$$\ddot{\theta}(t) = \frac{2\pi h}{T^2} \alpha \left(\sin \frac{2\pi(t - t_0)}{T} + \frac{1}{6} \sin \frac{6\pi(t - t_0)}{T} + \frac{1}{50} \sin \frac{10\pi(t - t_0)}{T} \right) \tag{15}$$

where $h = \theta_f - \theta_0$; θ_0 is the initial displacement; θ_f is the final displacement; T is the duration of the trajectory; t_0 is the initial time instant; t_1 is the final time instant; α is 0.9438.

The problem of finding an excitation trajectory $\theta^*(t)$ is formulated as

$$\theta^*(t) = \arg \min(\mathbf{J}) \tag{16}$$

where \mathbf{J} is an objective function to be determined afterwards, and $\theta_i^{\max} (^\circ)$, $\dot{\theta}_i^{\max} (^\circ s^{-1})$, and $\ddot{\theta}_i^{\max} (^\circ s^{-2})$ denote bounds on joint position, velocity and acceleration, respectively. The constraints in (17) are necessary to avoid discontinuities in displacement, velocity and acceleration at the start and endpoints in case $\theta_i(t_1) \neq 0$, $\dot{\theta}_i(t_1) \neq 0$, and $\ddot{\theta}_i(t_1) \neq 0$.

s.t.constraints

$$\begin{cases} |\theta_i| \leq \theta_i^{\max} = \text{displacement } i, t \\ |\dot{\theta}_i| \leq \dot{\theta}_i^{\max} = \text{velocity } i, t \\ |\ddot{\theta}_i| \leq \ddot{\theta}_i^{\max} = \text{acceleration } i, t \\ \theta_i(t_0) = \theta_i(t_1) = 0 \quad i, t \\ \dot{\theta}_i(t_0) = \dot{\theta}_i(t_1) = 0 \quad i, t \\ \ddot{\theta}_i(t_0) = \ddot{\theta}_i(t_1) = 0 \quad i, t \end{cases} \tag{17}$$

4. Testbed and signal processing

The ABB irb1600 industrial manipulator has been employed in this simulation experiment depicted in Figure 2(a), and its associated link frames are presented in Figure 2(b). The connection parameters of the robot are shown in Table 1. The ABB irb1600 has a serial structure with six rotation joints, as shown in Figure 3, making it ideal for glueing, arc welding, machine tending, material handling, deburring, and grinding tasks. In addition, the robot comes with the IRC5 controller, control software, and FlexPendant. However, the data gathered during identification, such as displacement, velocity, and acceleration, is prone to noise. Therefore, improving the accuracy of the parameter identification results requires reducing noise on (11) and (12). This study uses Savitzky-Golay smoothing filters to eliminate a noisy signal with a wide frequency range. The Savitzky-Golay filters (SGF) outperform traditional Finite Impulse Response (FIR) filters (Schafer, 2011), which are prone to filtering high-frequency information with the disturbance. Thus, they can help reduce the least-squares error when fitting a polynomial to noisy data frames. The sgolayfit function in MATLAB 2020a is used to implement the Savitzky-Golay filters (Schafer, 2011). The PC's specs include an Intel (R) Core(TM) i3-3110 M processor, 12GB of RAM, and a 1TB hard drive.

4.1. Results and discussion

Figure 4 shows that the reference trajectory for all joints is smooth, reducing the robot arm's shock and impact and ensuring the smooth operation of the ABB irb1600 robot. The black line represents the displacement after nonlinear least-squares identification with a disturbance. In contrast, the red line represents the displacement after applying the Savitzky-Golay smoothing filter. Furthermore, there is a significant disturbance in the third joint during excitations compared to the other joints.

Figure 5 demonstrates that the velocity for all joints is smooth, minimising the robot arm's shock and impact and assuring the smooth functioning of the ABB irb1600 robot. The black line shows the velocity following nonlinear least-squares identification with a disturbance. In contrast, the blue line indicates the velocity following the Savitzky-Golay smoothing filter. However, there is no substantial difference in the reference velocity between excitations employing the nonlinear least-square alone and those using the Savitzky-Golay smoothing filter.

Figure 6 shows that the reference acceleration for all joints is smooth, reducing the shock and effect on the robot arm and ensuring the smooth operation of the ABB irb1600 robot. The black line represents the acceleration after nonlinear least-squares identification with a disturbance, whereas the green line represents the acceleration after the Savitzky-Golay smoothing filter. However, the reference

Figure 4. Reference Trajectory

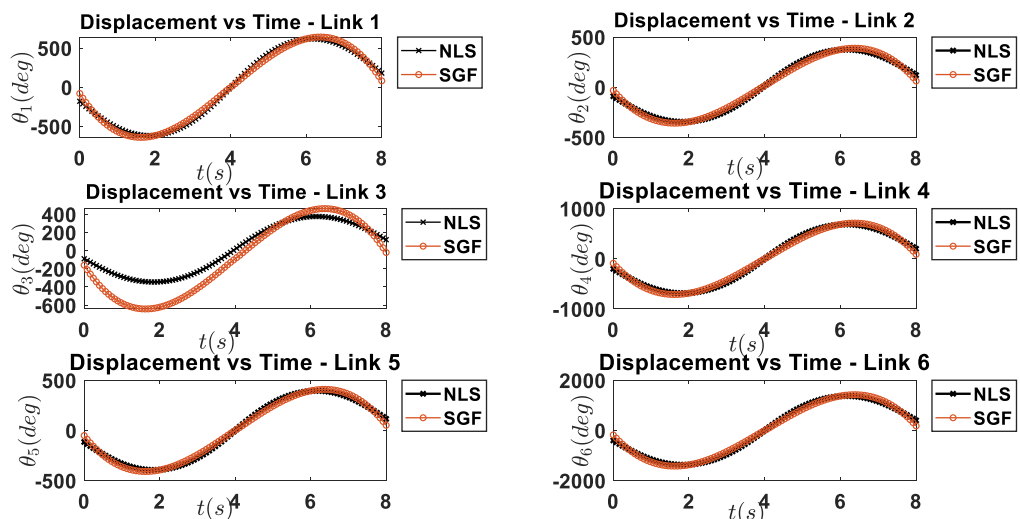


Figure 5. Reference velocity.

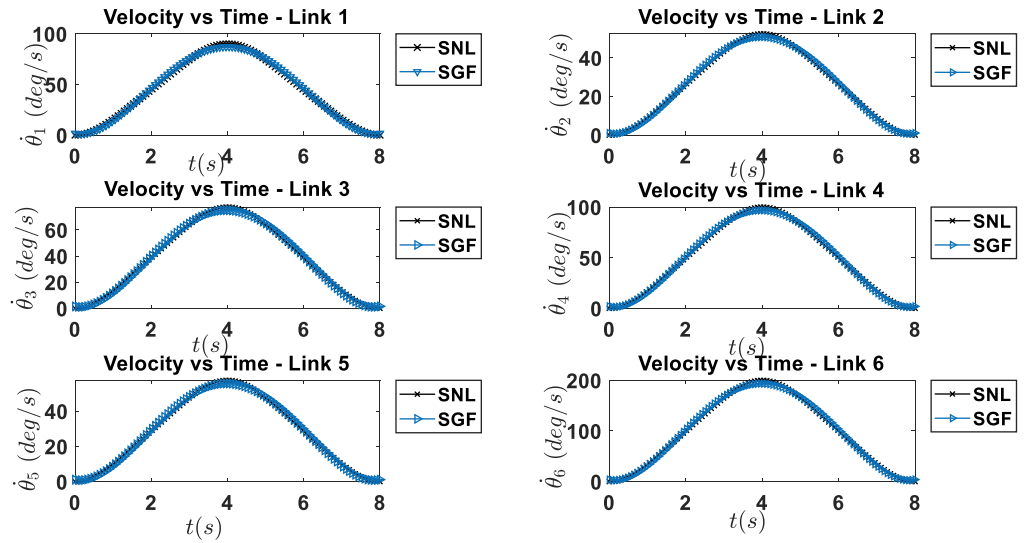


Figure 6. Reference acceleration.

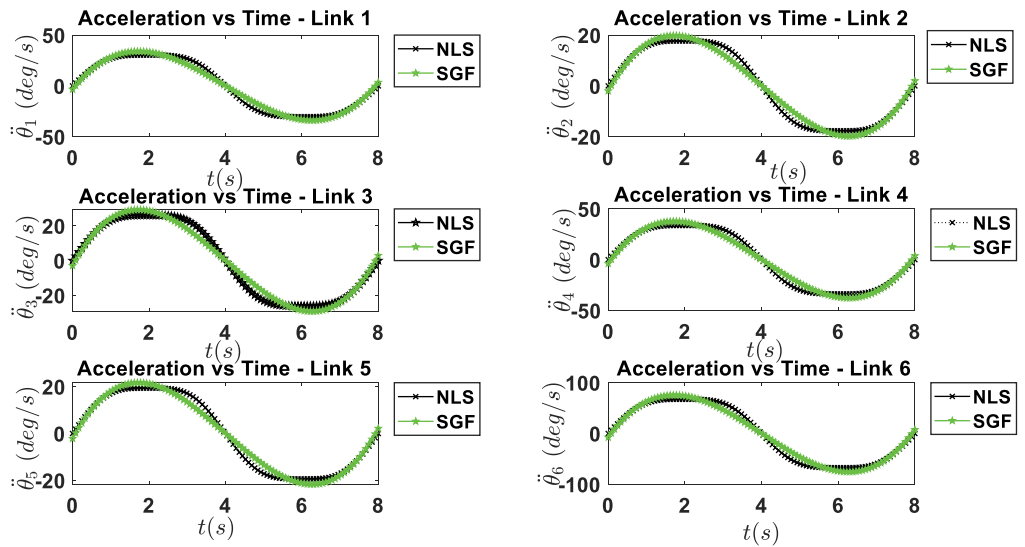


Figure 7. Reference torque.

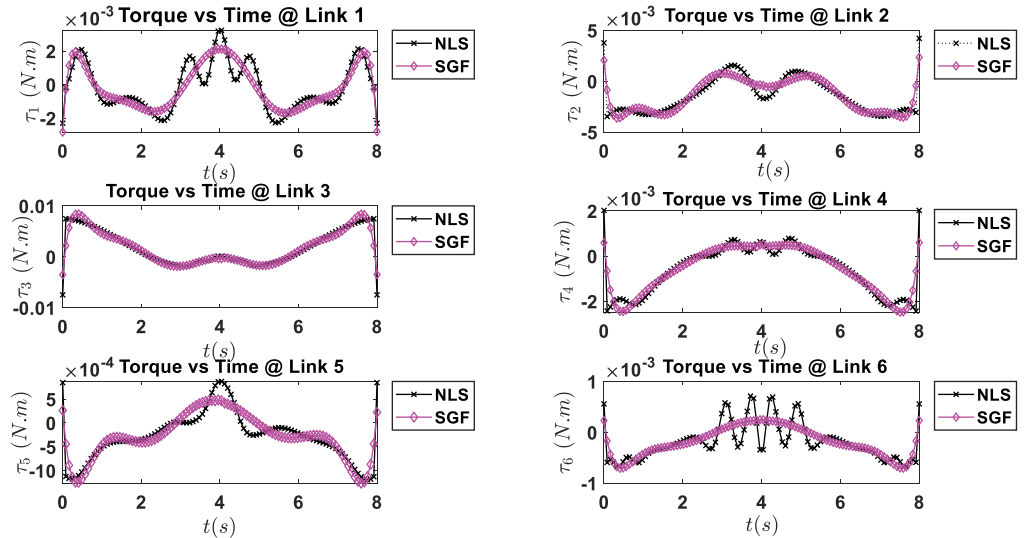


Table 2. The estimated dynamic parameters

Parameters	Values	Parameters	Values	Parameters	Values	Parameters	Values	Parameters	Values	Parameters	Values
$X_1 (Kg m^2)$	10.90	$X_{15} (Kg m^2)$	-0.35	$X_{29} (Kgs^{-1})$	$X_{43} (Kg m^2)$	0.013	$X_{57} (Kg m^2)$	-6.45e-9	$X_{71} (Kg m^2)$		7.7e-10
$X_2 (Kg m^2)$	-0.73	$X_{16} (Kg m^2)$	-0.034	$X_{30} (Kg m^2)$	$X_{44} (Kg m^2)$	-1.95e-9	$X_{58} (Kg m^2)$	5.86e-8	$X_{72} (Kg m^2)$		2.5e-5
$X_3 (Kg m^2)$	-0.73	$X_{17} (Kg m^2)$	0.72	$X_{31} (Kg m^2)$	$X_{45} (Kg m^2)$	-8.9e-5	$X_{59} (Kg m^2)$	0.007	$X_{73} (Kgs^{-1})$		-0.001
$X_4 (Kg m^2)$	-5.93	$X_{18} (Kg m^2)$	-1.59	$X_{32} (Kg m^2)$	$X_{46} (Kg m^2)$	-0.004	$X_{60} (Kg m^2)$	-0.0001	$X_{74} (Kgs^{-1})$		2.09e-5
$X_5 (Kg m^2)$	-1.43	$X_{19} (Kg m^2)$	-0.001	$X_{33} (Kg m^2)$	$X_{47} (Kg m^2)$	9.3e-5	$X_{61} (Kg m^2)$	1.87	$X_{75} (Kg m^2)$		0.033
$X_6 (Kg m^2)$	9.11	$X_{20} (Kg m^2)$	0.0026	$X_{34} (Kg m^2)$	$X_{48} (Kg m^2)$	-0.23	$X_{62} (Kg m^2)$	1.87	$X_{76} (Kg m^2)$		-8.31e-6
$X_7 (Kg m^2)$	1.56	$X_{21} (Kg m^2)$	-0.002	$X_{35} (Kg m^2)$	$X_{49} (Kg m^2)$	-0.137	$X_{63} (Kg m^2)$	1.9	$X_{77} (Kgs^{-1})$		-0.0006
$X_8 (Kg m^2)$	0.39	$X_{22} (Kg m^2)$	-0.46	$X_{36} (Kg m^2)$	$X_{50} (Kg m^2)$	0.10	$X_{64} (Kg m^2)$	-1.2e-7	$X_{78} (Kgs^{-1})$		4.21e-6
$X_9 (Kg m^2)$	0.40	$X_{23} (Kg m^2)$	-0.002	$X_{37} (Kg m^2)$	$X_{51} (Kg m^2)$	-0.34	$X_{65} (Kg m^2)$	2e-7			
$X_{10} (Kg m^2)$	0.29	$X_{24} (Kg m^2)$	0.0018	$X_{38} (Kg m^2)$	$X_{52} (Kg m^2)$	1.50	$X_{66} (Kg m^2)$	9.3e-10			
$X_{11} (Kg m^2)$	0.04	$X_{25} (Kg m^2)$	0.052	$X_{39} (Kg m^2)$	$X_{53} (Kg m^2)$	-0.01	$X_{67} (Kg m^2)$	2.8e-5			
$X_{12} (Kg m^2)$	-1.12	$X_{26} (Kg m^2)$	-9.5e-11	$X_{40} (Kg m^2)$	$X_{54} (Kg m^2)$	0.018	$X_{68} (Kgs^{-1})$	-0.0022			
$X_{13} (Kg m^2)$	-5.84	$X_{27} (Kg m^2)$	0.00013	$X_{41} (Kg m^2)$	$X_{55} (Kg m^2)$	-0.01	$X_{69} (Kgs^{-1})$	3.17e-5			
$X_{14} (Kg m^2)$	-0.34	$X_{28} (Kgs^{-1})$	0.001	$X_{42} (Kg m^2)$	$X_{56} (Kg m^2)$	-0.013	$X_{70} (Kg m^2)$	1.72			

Table 3. The standard deviation of the estimated torque

Joint #	Nonlinear least square	Savitzky-Golay filters
Joint 1	0.00142	0.0013
Joint 2	0.0017	0.0016
Joint 3	0.0035	0.0033
Joint 4	0.0011	0.0010
Joint 5	0.00051	0.00047
Joint 6	0.00036	0.00029

acceleration differs significantly between excitations using the nonlinear least-squares method alone and those utilising the Savitzky-Golay smoothing filter.

Figure 7 demonstrates that the reference torque for all joints is smooth, eliminating stress and effect on the robot arm and ensuring the ABB irb1600 robot operates smoothly. The black line depicts the acceleration following nonlinear least-squares identification with a disturbance, whereas the brown line represents the torque following the Savitzky-Golay smoothing filter. However, compared to other reference trajectories, the disruption during excitations has the most significant influence on the reference torque.

Table 2 shows the Symbolic expressions for the inertia parameters and the estimated values for the dynamic parameters using the Savitzky-Golay smoothing filter.

5. Conclusions

This study derived the robot dynamic model in its canonical version by employing the Euler-Lagrangian equation. A Freudenstein 1-3-5 trajectory, constructed based on Fourier series expansion, was employed to excite each link of the industrial robot. A slower acceleration rate is attained in the Freudenstein 1-3-5 profiles owing to the higher employment of Fourier series expansion terms. At the same time, limits were enforced to prevent discontinuities in displacement, velocity and acceleration at the start and ends. Nonlinear least-squares based on the Levenberg-Marquart approach was used to find the dynamic parameters of a six-degree-of-freedom ABB irb1600 robot. To boost the identification scheme’s performance, we utilise Savitzky-Golay smoothing filters to eliminate a noisy signal with a significant frequency spread. The standard deviation of the torque is compared in Table 3 using nonlinear least squares and Savitzky-Golay filters. The decreased standard deviation values produced with the Savitzky-Golay filters suggest that the values are closer to the mean, which is a desirable attribute.

Acknowledgements

The authors revealed that the research was funded in part by the Technology Innovation Agency (TIA) of South Africa, the Gibela Rail Transport Consortium (GRTC), the National Research Foundation (NRF grant 123575), and Tshwane University of Technology (TUT).

Funding

This work was supported by the National Research Foundation (NRF grant 123575), and Tshwane University of Technology (TUT). [(NRF grant 123575).

Author details

John Ogbemhe¹
 E-mail: johnogbemhe@gmail.com
 ORCID ID: <http://orcid.org/0000-0002-7578-0078>
 Khumbulani Mpofu¹
 ORCID ID: <http://orcid.org/0000-0003-3429-7677>
 Mabolaya Makakabye¹

¹ Department of Industrial Engineering, Tshwane University of Technology, Pretoria West 0183 Pretoria, South Africa.

Disclosure statement

No potential conflict of interest was reported by the author(s).

List of symbols

W	weighting matrix.
σ_{yi}	measurement error.
$\theta^*(t)$	Excitation trajectory
J	Objective function
$\dot{y}(t_i; p)$	the model function of an independent variable t
λ	Damping parameter.
h	The initial displacement
$\theta_i(t)$	Vector position of the i^{th} joint.
$\dot{\theta}_i(t)$	Vector of the velocity of the i^{th} joint.
$\ddot{\theta}_i(t)$	Vector of acceleration of the i^{th} joint.
$M(\theta)$	Inertia matrix of the industrial robot.
$H(\theta, \dot{\theta})$	Coriolis terms.
$G(\theta)$	Gravity forces terms.
	Friction forces.

$\tau_f(t)$	
$\tau(t)$	Joint torque vector
f_v	$n \times n$ diagonal matrices representing viscous friction parameters
f_c	$n \times n$ diagonal matrices representing Coulomb friction parameters
$\text{sgn}(\cdot)$	Sign function.
m_i	Mass of the i^{th} joint.
a_i	Centre of the mass i^{th} joint.
l_i	Length of the i^{th} link.
$Y(\theta, \dot{\theta}, \ddot{\theta})$	Regressor matrix.
X_s	Standard parameter vector
g	Acceleration due to gravity.
I_{xx}	Moment of inertia in the xx plane of the i^{th} link.
I_{xy}	Moment of inertia in the xy plane of the i^{th} link.
I_{xz}	Moment of inertia in the xz plane of the i^{th} link.
I_{yy}	Moment of inertia in the yy plane of the i^{th} link.
I_{zz}	Moment of inertia in the zz plane of the i^{th} link.
I_{yz}	Moment of inertia in the yz plane of the i^{th} link.

Citation information

Cite this article as: Robot dynamic model: freudenstein-based optimal trajectory and parameter identification, John Ogbehe, Khumbulani Mpofu & Mabolaya Mokakabye, *Cogent Engineering* (2022), 9: 2046682.

References

- Biagiotti, L., & Melchiorri, C. (2008). *Trajectory planning for automatic machines and robots* (Germany: Springer Science & Business Media).
- Calanca, A., Capisani, L. M., Ferrara, A., & Magnani, L. (2010). MIMO closed loop identification of an industrial robot. *IEEE Transactions on Control Systems Technology*, 19(5), 1214–1224. <https://doi.org/10.1109/TCST.2010.2077294>
- Carvalho Bittencourt, A. (2014). *Modeling and diagnosis of friction and wear in industrial robots*. Linköping University Electronic Press.
- Chiddarwar, S. S., & Babu, N. R. (2012). Optimal trajectory planning for industrial robot along a specified path with payload constraint using trigonometric splines. *International Journal of Automation and Control*, 6(1), 39–65. <https://doi.org/10.1504/IJAAC.2012.045439>
- Ding, L., Wu, H., Yao, Y., & Yang, Y. (2015). Dynamic model identification for 6-DOF industrial robots. *Journal of Robotics*, 2015, 1–9. <https://doi.org/10.1155/2015/471478>
- Gao, G., Sun, G., Na, J., Guo, Y., & Wu, X. (2018). Structural parameter identification for 6 DOF industrial robots. *Mechanical Systems and Signal Processing*, 113, 145–155. <https://doi.org/10.1016/j.ymssp.2017.08.011>
- Gautier, M., & Briot, S. (2013). *Dynamic parameter identification of a 6 DOF industrial robot using power model*. Paper presented at the 2013 IEEE international conference on robotics and automation 6-10 May 2013 (IEEE) Karlsruhe, Germany.
- Gavin, H. P. 2019. The Levenberg-Marquardt algorithm for nonlinear least squares curve-fitting problems. Department of Civil and Environmental Engineering, Duke University. (281), 1–19. <http://people.duke.edu/~Hpgavin/ce/lm.pdf>
- Hao, L., Pagani, R., Beschi, M., & Legnani, G. (2021). Dynamic and friction parameters of an industrial robot: identification, comparison and repetitiveness analysis. *Robotics*, 10(1), 49. <https://doi.org/10.3390/robotics10010049>
- Hardeman, T. (2008). *Modelling and identification of industrial robots including drive and joint flexibilities*. Universiteit Twente.
- Hayat, A. A., Abhishek, V., & Saha, S. K. Department of Mechanical Engineering, IIT Kanpur 2015 manipulator: comparison between cad and actual parameters (Kanpur: iNaCoMM) *Dynamic identification of manipulator: comparison between cad and actual parameters*.
- Huang, J., Hu, P., Wu, K., & Zeng, M. (2018). Optimal time-jerk trajectory planning for industrial robots. *Mechanism and Machine Theory*, 121, 530–544. <https://doi.org/10.1016/j.mechmachtheory.2017.11.006>
- Jin, J., & Gans, N. (2015). Parameter identification for industrial robots with a fast and robust trajectory design approach. *Robotics and Computer-Integrated Manufacturing*, 31, 21–29. <https://doi.org/10.1016/j.rcim.2014.06.004>
- Kozłowski, K. R. (2012). *Modelling and identification in robotics*. Springer Science & Business Media.
- Kröger, T. (2010). On-line trajectory generation in robotic systems, volume 58. *Of Springer Tracts in Advanced Robotics English* 58 1610-7438 doi:<https://doi.org/10.1007/978-3-642-05175-3>
- Liu, S.-P., Ma, Z.-Y., Chen, J.-L., Cao, J.-F., Fu, Y., & Li, S.-Q. (2021). An improved parameter identification method of redundant manipulator. *International Journal of Advanced Robotic Systems*, 18(2), 17298814211002118. <https://doi.org/10.1177/17298814211002118>
- Madsen, E. (2020). *Joint dynamics and adaptive feedforward control of lightweight industrial robots* ISBN-13 (15) 978-87-7507-485-3 <https://doi.org/10.7146/aul.384>
- Nguyen, M.-T., & Huang, J.-L. (2019). *Smooth and time optimal trajectory planning for industrial robot using a single polynomial*. Paper presented at the international conference on engineering research and applications 24-26 October 2019. <https://icera2019.ru/> Moscow, Russia.
- Ogbehe, J., & Mpofu, K. (2015). Towards achieving a fully intelligent robotic arc welding: A review. *Industrial Robot: An International Journal*, 42(5), 475–484. <https://doi.org/10.1108/IR-03-2015-0053>
- Ogbehe, J., Mpofu, K., & Tlale, N. (2019). Optimal trajectory scheme for robotic welding along complex joints using a hybrid multi-objective genetic algorithm. *IEEE Access*, 7, 158753–158769. <https://doi.org/10.1109/ACCESS.2019.2950561>
- Pagani, R., Legnani, G., Incerti, G., & Gheza, M. (2020). Evaluation and modeling of the friction in robotic joints considering thermal effects. *Journal of Mechanisms and Robotics*, 12(2). <https://doi.org/10.1115/1.4045939>
- Rackl, W., Lampariello, R., & Hirzinger, G. (2012). *Robot excitation trajectories for dynamic parameter estimation using optimized B-splines*. Paper presented at the 2012 IEEE international conference on robotics and automation 14-18 May 2012 (USA: IEEE)doi:<https://doi.org/10.1109/ICRA.2012.6225279> Saint Paul, MN, USA.
- Rymansaub, Z., Iravani, P., & Sahinkaya, M. N. (2013). *Exponential trajectory generation for point to point motions*. Paper presented at the 2013 IEEE/ASME international conference on advanced intelligent mechatronics 9-12 July 2013 (IEEE)doi:<https://doi.org/10.1109/AIM.2013.6584209> Wollongong, NSW, Australia.

- Schafer, R. W. (2011). What is a Savitzky-Golay filter?[lecture notes]. *IEEE Signal Processing Magazine*, 28(4), 111–117. <https://doi.org/10.1109/MSP.2011.941097>
- Shang, W., & Cong, S. (2015). OPTIMAL CALIBRATION AND IDENTIFICATION OF A 2-DOF PARALLEL MANIPULATOR WITH REDUNDANT ACTUATION. *International Journal of Robotics and Automation*, 30(5) 333–344). <https://doi.org/10.2316/Journal.206.2015.5.206-4391>
- Siciliano, B., & Khatib, O. (2008). *Springer handbook of robotics*. Springer Science & Business Media.
- song, Q., Li, S., Bai, Q., Yang, J., Zhang, A., Zhang, X., & Zhe, L. (2021). Trajectory planning of robot manipulator based on RBF neural network. *Entropy*, 23(9), 1207. <https://doi.org/10.3390/e23091207>
- Sweet, L., & Good, M. (1985). Redefinition of the robot motion-control problem. *IEEE Control Systems Magazine*, 5(3), 18–25. <https://doi.org/10.1109/MCS.1985.1104955>
- Villagrossi, E., Legnani, G., Pedrocchi, N., Vicentini, F., Tosatti, L. M., Abbà, F., & Bottero, A. (2014). Robot dynamic model identification through excitation trajectories minimizing the correlation influence among essential parameters. Paper presented at the 2014 11th international conference on informatics in control, automation and robotics (ICINCO) 1-3 Sept. 2014 (IEEE)doi:<https://doi.org/10.5220/0005060704750482> Vienna, Austria.
- Wu, J., Wang, J., & You, Z. (2010). An overview of dynamic parameter identification of robots. *Robotics and Computer-Integrated Manufacturing*, 26(5), 414–419. <https://doi.org/10.1016/j.rcim.2010.03.013>
- Zollo, L., Lopez, E., Spedalieri, L., Aracil, N. G., & Guglielmelli, E. (2015). Identification of dynamic parameters for robots with elastic joints. *Advances in Mechanical Engineering*, 7(2), 843186. <https://doi.org/10.1155/2014/843186>

Appendix

Table A1. The meaning of the inertia parameters in terms of physics		
Parameter	Meaning	Unit
X_1	$2(lz_1 + lz_2 + lz_3 + lz_4 + lz_5 + lz_6)$	Kgm ²
X_2	$m_6 \left(\frac{\beta_1^2 + 2(\alpha_1\beta_1 + \alpha_1\beta_2 + \alpha_1\beta_3 + \alpha_1\beta_4 + \alpha_1\beta_5 + \alpha_1\beta_6) + \alpha_1^2 + \alpha_2^2 + \alpha_3^2 + \alpha_4^2 + \alpha_5^2 + \alpha_6^2}{+2(-\alpha_1\alpha_2 + \alpha_1\alpha_3 + \alpha_1\alpha_4 + \alpha_1\alpha_5 + \alpha_1\alpha_6 + \alpha_2\alpha_3 + \alpha_2\alpha_4 + \alpha_2\alpha_5 + \alpha_2\alpha_6 + \alpha_3\alpha_4 + \alpha_3\alpha_5 + \alpha_3\alpha_6 + \alpha_4\alpha_5 + \alpha_4\alpha_6 + \alpha_5\alpha_6)} \right)$	Kgm ²
X_3	$m_5 \left(\frac{\beta_1 + 2(\alpha_1\beta_1 + \alpha_1\beta_2 + \alpha_1\beta_3 + \alpha_1\beta_4 + \alpha_1\beta_5 + \alpha_1\beta_6) + \alpha_1^2 + \alpha_2^2 + \alpha_3^2 + \alpha_4^2 + \alpha_5^2}{+2(\alpha_1\alpha_2 + \alpha_1\alpha_3 + \alpha_1\alpha_4 + \alpha_1\alpha_5 + \alpha_1\alpha_6 + \alpha_2\alpha_3 + \alpha_2\alpha_4 + \alpha_2\alpha_5 + \alpha_2\alpha_6 + \alpha_3\alpha_4 + \alpha_3\alpha_5 + \alpha_3\alpha_6 + \alpha_4\alpha_5 + \alpha_4\alpha_6 + \alpha_5\alpha_6)} \right)$	Kgm ²
X_4	$m_4(2(\alpha_1\beta_1 + \alpha_1\beta_2 + \alpha_1\beta_3 + \alpha_1\beta_4 + \alpha_1\beta_5 + \alpha_1\beta_6) + \alpha_1^2 + 2(\alpha_1\alpha_2 + \alpha_1\alpha_3 + \alpha_1\alpha_4))$	Kgm ²
X_5	$m_3(\beta_1^2 + 2\alpha_1\beta_1 + 2\alpha_1\beta_2 + \alpha_1^2 + \alpha_2^2 + 2\alpha_2\alpha_3)$	Kgm ²
X_6	$m_2(\beta_1^2 + 2\alpha_1\beta_1 + \alpha_1^2)$	Kgm ²
X_7	$2(lz_2 + lz_3 + lz_4 + lz_5 + lz_6)$	Kgm ²
X_8	$m_6 \left(\frac{(h_1(\alpha_1 + \alpha_2 + \alpha_3 + \alpha_4 + \alpha_5 + \alpha_6) + \alpha_1^2 + \alpha_2^2 + \alpha_3^2 + \alpha_4^2 + \alpha_5^2 + \alpha_6^2)}{+2(\alpha_1\alpha_2 + \alpha_1\alpha_3 + \alpha_1\alpha_4 + \alpha_1\alpha_5 + \alpha_1\alpha_6 + \alpha_2\alpha_3 + \alpha_2\alpha_4 + \alpha_2\alpha_5 + \alpha_2\alpha_6 + \alpha_3\alpha_4 + \alpha_3\alpha_5 + \alpha_3\alpha_6 + \alpha_4\alpha_5 + \alpha_4\alpha_6 + \alpha_5\alpha_6)} \right)$	Kgm ²
X_9	$m_5(h_1(\alpha_1 + \alpha_2 + \alpha_3 + \alpha_4 + \alpha_5) + 2(\alpha_1\alpha_2 + \alpha_1\alpha_3 + \alpha_1\alpha_4 + \alpha_1\alpha_5 + \alpha_2\alpha_3 + \alpha_2\alpha_4 + \alpha_2\alpha_5) + \alpha_1^2 + \alpha_2^2 + \alpha_3^2 + \alpha_4^2 + \alpha_5^2)$	Kgm ²
X_{10}	$m_4(h_1(\alpha_1 + \alpha_2 + \alpha_3 + \alpha_4) + \alpha_1^2 + \alpha_2^2 + \alpha_3^2 + \alpha_4^2 + 2(\alpha_1\alpha_2 + \alpha_1\alpha_3 + \alpha_1\alpha_4))$	Kgm ²
X_{11}	$m_3(h_1(\alpha_1 + \alpha_2 + \alpha_3) + \alpha_1^2 + \alpha_2^2 + 2\alpha_2\alpha_3)$	Kgm ²
X_{12}	$m_2(\alpha_1\beta_1 + \alpha_1^2)$	Kgm ²
X_{13}	$2(lz_2 + lz_3 + lz_4 + lz_5 + lz_6)$	Kgm ²
X_{14}	$m_6 \left(\frac{(h_1(\alpha_1 + \alpha_2 + \alpha_3 + \alpha_4 + \alpha_5 + \alpha_6) + \alpha_1^2 + \alpha_2^2 + \alpha_3^2 + \alpha_4^2 + \alpha_5^2 + \alpha_6^2)}{+2(\alpha_1\alpha_2 + \alpha_1\alpha_3 + \alpha_1\alpha_4 + \alpha_1\alpha_5 + \alpha_1\alpha_6 + \alpha_2\alpha_3 + \alpha_2\alpha_4 + \alpha_2\alpha_5 + \alpha_2\alpha_6 + \alpha_3\alpha_4 + \alpha_3\alpha_5 + \alpha_3\alpha_6 + \alpha_4\alpha_5 + \alpha_4\alpha_6 + \alpha_5\alpha_6)} \right)$	Kgm ²
X_{15}	$m_5(h_1(\alpha_1 + \alpha_2 + \alpha_3 + \alpha_4 + \alpha_5) + \alpha_1^2 + \alpha_2^2 + \alpha_3^2 + \alpha_4^2 + \alpha_5^2 + 2(\alpha_1\alpha_2 + \alpha_1\alpha_3 + \alpha_1\alpha_4 + \alpha_1\alpha_5 + \alpha_2\alpha_3 + \alpha_2\alpha_4 + \alpha_2\alpha_5) + 2\alpha_2\alpha_3)$	Kgm ²
X_{16}	$m_4(h_1(\alpha_1 + \alpha_2 + \alpha_3) + \alpha_1^2 + \alpha_2^2 + \alpha_3^2 + \alpha_4^2 + 2\alpha_3\alpha_4)$	Kgm ²
X_{17}	$m_3(\alpha_1\beta_1 + \alpha_1^2 + \alpha_2^2)$	Kgm ²
X_{18}	$2(lz_2 + lz_3 + lz_4 + lz_5 + lz_6)$	Kgm ²
X_{19}	$m_6 \left(\frac{(h_1(\alpha_1 + \alpha_2 + \alpha_3 + \alpha_4) + \alpha_1^2 + \alpha_2^2 + \alpha_3^2 + \alpha_4^2 + \alpha_5^2 + \alpha_6^2)}{+2(\alpha_1\alpha_2 + \alpha_1\alpha_3 + \alpha_1\alpha_4 + \alpha_1\alpha_5 + \alpha_1\alpha_6 + \alpha_2\alpha_3 + \alpha_2\alpha_4 + \alpha_2\alpha_5 + \alpha_2\alpha_6 + \alpha_3\alpha_4 + \alpha_3\alpha_5 + \alpha_3\alpha_6 + \alpha_4\alpha_5 + \alpha_4\alpha_6 + \alpha_5\alpha_6)} \right)$	Kgm ²
X_{20}	$m_5(h_1(\alpha_1 + \alpha_2 + \alpha_3) + \alpha_1^2 + \alpha_2^2 + \alpha_3^2 + \alpha_4^2 + \alpha_5^2 + 2\alpha_4\alpha_5)$	Kgm ²
X_{21}	$m_4(\alpha_1\beta_1 + \alpha_1^2 + \alpha_2\alpha_4 + \alpha_1\alpha_4)$	Kgm ²
X_{22}	$2(lz_2 + lz_3)$	Kgm ²
X_{23}	$m_6(h_1(\alpha_1 + \alpha_2) + \alpha_1^2 + \alpha_2^2 + \alpha_3\alpha_5 + \alpha_2\alpha_6 + \alpha_3\alpha_5 + \alpha_4\alpha_5 + \alpha_4\alpha_6 + \alpha_5\alpha_6 + 2\alpha_5\alpha_6)$	Kgm ²
X_{24}	$m_5(\alpha_1\beta_1 + \alpha_1^2 + \alpha_2\alpha_5 + \alpha_1\alpha_5 + \alpha_1\alpha_5)$	Kgm ²
X_{25}	$2lz_6$	Kgm ²
X_{26}	$m_6(\alpha_1\beta_1 + \alpha_1^2 + \alpha_2\alpha_5 + \alpha_1\alpha_5 + \alpha_1\alpha_5)$	Kgm ²
X_{27}	$\left(\frac{\alpha_1 m_1 + \alpha_2(m_2 + m_3 + m_4 + m_5 + m_6) + \alpha_3(m_3 + m_4 + m_5 + m_6) + \alpha_4(m_4 + m_5 + m_6)}{+ \alpha_5(m_5 + m_6) + \alpha_6 m_6 + h_1(m_2 + m_3 + m_4 + m_5 + m_6)} \right)$	Kgm ²
X_{28}	f_{15}	Kgs ⁻¹

(Continued)

Table A1. (Continued)

X ₂₉	f_{1v}	Kgs^{-1}
X ₃₀	$m_6 (a_1^2 + a_2^2 + a_3^2 + a_4^2 + a_5^2 + a_6^2 + 2(a_2a_3 + a_2a_4 + a_2a_5 + a_2a_6 + a_3a_4 + a_3a_5 + a_3a_6 + a_4a_5 + a_4a_6 + a_5a_6))$	Kgm^2
X ₃₁	$m_5 (a_2^2 + a_3^2 + a_4^2 + a_5^2 + 2(a_2a_3 + a_2a_4 + a_2a_5 + a_2a_6 + a_3a_4 + a_3a_5 + a_3a_6))$	Kgm^2
X ₃₂	$m_4 (a_2^2 + a_3^2 + a_4^2 + 2(a_2a_3 + a_2a_4 + a_2a_5))$	Kgm^2
X ₃₃	$m_3 (a_2^2 + a_3^2 + 2a_2a_3)$	Kgm^2
X ₃₄	$m_2 (a_2^2)$	Kgm^2
X ₃₅	$m_6 (a_1^2 + a_2^2 + a_3^2 + a_4^2 + a_5^2 + a_6^2 + 2(a_2a_3 + a_2a_4 + a_2a_5 + a_2a_6 + a_3a_4 + a_3a_5 + a_3a_6 + a_4a_5 + a_4a_6 + a_5a_6))$	Kgm^2
X ₃₆	$m_5 (a_2^2 + a_3^2 + a_4^2 + a_5^2 + 2(a_2a_3 + a_2a_4 + a_2a_5 + a_2a_6 + a_3a_4 + a_3a_5 + a_3a_6))$	Kgm^2
X ₃₇	$m_4 (a_2^2 + a_3^2 + a_4^2 + 2a_2a_3)$	Kgm^2
X ₃₈	$m_3 (a_2^2 + a_3^2)$	Kgm^2
X ₃₉	$m_6 (a_1^2 + a_2^2 + a_3^2 + a_4^2 + a_5^2 + a_6^2 + a_1a_2 + a_1a_3 + a_1a_4 + a_1a_5 + a_1a_6 + 2(a_2a_3 + a_2a_4 + a_2a_5 + a_2a_6 + a_3a_4 + a_3a_5 + a_3a_6))$	Kgm^2
X ₄₀	$m_5 (a_2^2 + a_3^2 + a_4^2 + a_5^2 + 2a_2a_3)$	Kgm^2
X ₄₁	$m_4 (a_2^2 + a_3^2 + a_4^2)$	Kgm^2
X ₄₂	$m_6 (a_1^2 + a_2^2 + a_3^2 + a_4^2 + a_5^2 + a_6^2 + a_1a_2 + a_1a_3 + a_1a_4 + a_1a_5 + a_1a_6 + 2a_2a_3)$	Kgm^2
X ₄₃	$m_5 (a_2^2 + a_3^2 + a_4^2 + a_5^2)$	Kgm^2
X ₄₄	$m_6 (a_1^2 + a_2^2 + a_3^2 + a_4^2 + a_5^2 + a_6^2 + a_1a_2)$	Kgm^2
X ₄₅	$(a_2m_6 + a_3(m_3 + m_4 + m_5) + a_4(m_5 + m_6))$	Kgm^2
X ₄₆	f_{2s}	Kgs^{-1}
X ₄₇	f_{1v}	Kgs^{-1}
X ₄₈	$m_6 (a_1^2 + a_2^2 + a_3^2 + a_4^2 + 2(a_2a_3 + a_2a_4 + a_2a_5 + a_2a_6 + a_3a_4 + a_3a_5 + a_3a_6 + a_4a_5 + a_4a_6 + a_5a_6))$	Kgm^2
X ₄₉	$m_5 (a_2^2 + a_3^2 + a_4^2 + 2(a_2a_3 + a_2a_4 + a_2a_5))$	Kgm^2
X ₅₀	$m_4 (a_2^2 + a_3^2 + 2a_2a_3)$	Kgm^2
X ₅₁	$m_3 (a_2^2)$	Kgm^2
X ₅₂	$m_6 (a_1^2 + a_2^2 + a_3^2 + a_4^2 + a_5^2 + a_6^2 + 2(a_2a_3 + a_2a_4 + a_2a_5 + a_2a_6 + a_3a_4 + a_3a_5 + a_3a_6))$	Kgm^2
X ₅₃	$m_5 (a_2^2 + a_3^2 + a_4^2 + a_5^2 + 2a_2a_3)$	Kgm^2
X ₅₄	$m_4 (a_2^2 + a_3^2)$	Kgm^2
X ₅₅	$m_6 (a_1^2 + a_2^2 + a_3^2 + a_4^2 + a_5^2 + a_6^2 + a_1a_2 + a_1a_3 + a_1a_4 + a_1a_5 + a_1a_6 + 2a_2a_3)$	Kgm^2
X ₅₆	$m_5 (a_2^2 + a_3^2 + a_4^2)$	Kgm^2
X ₅₇	$m_6 (a_1^2 + a_2^2 + a_3^2 + a_4^2 + a_5^2 + a_6^2 + a_1a_2 + a_1a_3 + a_1a_4 + a_1a_5 + a_1a_6 + 2a_2a_3)$	Kgm^2
X ₅₈	$(a_1(m_3 + m_4 + m_5 + m_6) + a_2(m_4 + m_5 + m_6) + a_3(m_5 + m_6) + a_4(m_6))$	Kgm^2
X ₅₉	f_{2s}	Kgs^{-1}
X ₆₀	f_{1v}	Kgs^{-1}
X ₆₁	$m_6 (a_1^2 + a_2^2 + a_3^2 + 2a_2a_3 + 2a_2a_4 + 2a_2a_5 + 2a_2a_6)$	Kgm^2
X ₆₂	$m_5 (a_2^2 + a_3^2 + 2a_2a_3)$	Kgm^2
X ₆₃	$a_1^2 m_4$	Kgm^2

(Continued)

Table A1. (Continued)

X_{e4}	$m_6(a_2^2 + a_3^2 + a_4a_5 + 2a_3a_6)$	Kgm^2
X_{e5}	$m_5(a_2^2 + a_3a_5)$	Kgm^2
X_{e6}	$m_6(a_2^2 + a_3a_6 + a_3a_6)$	Kgm^2
X_{e7}	$(a_4am_4 + a_4(m_5 + m_6) + a_5(m_5 + m_6) + a_6m_6)$	Kgm^2
X_{e8}	f_{fs}	Kgs^{-1}
X_{e9}	f_{fv}	Kgs^{-1}
X_{f0}	$(a_2^2m_5 + a_2^2m_6 + a_2^2m_6 + 2a_3a_6m_6)$	Kgm^2
X_{f1}	$m_6(a_2^2 + a_3a_6)$	Kgm^2
X_{f2}	$(a_5m_5 + a_5m_6 + a_6m_6)$	Kgm^2
X_{f3}	f_{fs}	Kgs^{-1}
X_{f4}	f_{fv}	Kgs^{-1}
X_{f5}	$a_2^2m_6$	Kgm^2
X_{f6}	$a_3a_6m_6$	Kgm^2
X_{f7}	f_{fs}	Kgs^{-1}
X_{f8}	f_{fv}	Kgs^{-1}

m is the mass, and a are link length and centre of mass; f_v and f_s represents viscous and Coulomb friction parameters respectively and g is the acceleration due to gravity.



© 2022 The Author(s). This open access article is distributed under a Creative Commons Attribution (CC-BY) 4.0 license.

You are free to:

Share — copy and redistribute the material in any medium or format.

Adapt — remix, transform, and build upon the material for any purpose, even commercially.

The licensor cannot revoke these freedoms as long as you follow the license terms.

Under the following terms:

Attribution — You must give appropriate credit, provide a link to the license, and indicate if changes were made.

You may do so in any reasonable manner, but not in any way that suggests the licensor endorses you or your use.

No additional restrictions

You may not apply legal terms or technological measures that legally restrict others from doing anything the license permits.



Cogent Engineering (ISSN: 2331-1916) is published by Cogent OA, part of Taylor & Francis Group.

Publishing with Cogent OA ensures:

- Immediate, universal access to your article on publication
- High visibility and discoverability via the Cogent OA website as well as Taylor & Francis Online
- Download and citation statistics for your article
- Rapid online publication
- Input from, and dialog with, expert editors and editorial boards
- Retention of full copyright of your article
- Guaranteed legacy preservation of your article
- Discounts and waivers for authors in developing regions

Submit your manuscript to a Cogent OA journal at www.CogentOA.com

